Effects of surface charging treatment on outer and inner surfaces of a nanoporous carbon

Weiyi Lu
Department of Structural Engineering, University of California–San Diego, La Jolla, California 92093-0085

Aijie Han
Department of Chemistry, University of Texas–Pan America, Edinburg, Texas 78539

Taewan Kim and Hyuck Lim
Program of Materials Science & Engineering, University of California–San Diego, La Jolla, California 92093

Yu Qiao[a)]
Department of Structural Engineering, University of California–San Diego, La Jolla, California 92093-0085; and Program of Materials Science & Engineering, University of California–San Diego, La Jolla, California 92093

(Received 3 February 2009; accepted 24 March 2009)

As the outer surface of a nanoporous carbon is treated with 16-mercaptohexadecanoic acid, the carbon particles can form a stable suspension in water. When the water phase is compressed, the liquid infiltration behavior in the nanopores becomes significantly different from that of untreated material, suggesting that the inner surface is also modified. After the treatment, the infiltration pressure does not decrease. Therefore, the chain configurations at the inner and outer surfaces must be different, which explains the variations in infiltration pressure and volume.

I. INTRODUCTION

In the past, nanoporous materials were mainly used in the biological and chemical fields for catalysis, absorption and adsorption, separation and purification, and so on.[1–3] One of their most attractive properties is the ultra-large surface area, typically at the level of 10^2–10^3 m^2/g,[4,5] which can greatly amplify beneficial surface chemical reactions (e.g., for catalysis) and/or surface physical processes (e.g., for absorption).

Recently, the application of nanoporous materials was extended to mechanical systems, such as nanoporous energy absorption systems (NEAS).[6–8] A NEAS contains two phases: a nanoporous phase, which is often in the form of micrometer (μm) sized particles, and a liquid phase in which the nanoporous particles are immersed. The properties of the inner surfaces of nanopores must be appropriately controlled so that the effective solid-liquid interfacial tension, γ_{sl}, is larger than $\gamma_s + \gamma_l$, where γ_s and γ_l are the effective surface tensions of the nanopore wall and the liquid, respectively; that is, work needs to be done to expose the nanopore surface to the liquid. Thus, at rest the repelling effect of the nanopore surfaces would keep the liquid phase out of the nanopores. As external pressure is applied, the liquid can be compressed into the nanopores, accompanied by a large increase in system free energy, the amount of which is proportional to the total surface area. Such a system is effectively a compressible liquid, which is relevant to advanced damping and protection devices, such as vehicle bumpers, liquid armors, and damping stages, among others.[9,10]

Among the large number of nanoporous materials that have been investigated for NEAS, nanoporous carbons have received wide attention.[11] Unlike many other nanoporous materials, such as silicas and aluminas, which must be synthesized through sophisticated templating procedures, nanoporous carbons can be directly produced through carbonization of organic materials (e.g., carbon blacks and activated carbons), and activated by relatively simple hydrothermal treatments. Therefore, they are cost-efficient. Their nanopore sizes can be controlled in a wide range from less than 1 nm to the sub-μm level. The nanopores can be either open or closed, interconnected or isolated, and one dimensional or three dimensional. The thermal and electrical properties can also be adjusted over broad spectra. The surface areas and pore volumes of nanoporous carbons are often larger than those of other nanoporous materials. Previous experimental data have validated that they can be used to produce high-energy-density NEAS.[12–14]

[a)]Address all correspondence to this author.
e-mail: yqiao@ucsd.edu
DOI: 10.1557/JMR.2009.0296

 © 2009 Materials Research Society

One problem of nanoporous carbon based NEAS is that, because the carbon phase and the liquid phase are often of different mass densities, the carbon particles may not be stably suspended. Shortly after an NEAS is placed at rest, the lightweight carbon particles can float on the surface, and the system becomes heterogeneous. While under a uniform loading as long as the nanopores are accessible the overall liquid infiltration behavior and the energy absorption capacity are not affected, the phase separation can be problematic if the external loading is dynamic, and impose tremendous challenges to quality control in materials preparation and packaging.

A promising method that can stabilize liquid suspensions is to surface charge the particles; that is, if permanent electric charges, for example, charged surface groups, are decorated on the particle surfaces, they tend to repel each other and thus aggregation can be suppressed. While surface electrostatics may be generated physically by placing two different materials together,[15] to produce stable surface charges in a liquid medium, chemical surface treatment is usually the most robust method. By grafting charged molecules, often organic chains with charged end groups, the surface properties of the solid can be controlled in desired ranges. Note that a charged surface usually attracts water molecules and is effectively hydrophilic. For the NEAS, when the outer particle surfaces are modified, the inner surface must be maintained hydrophobic.

II. EXPERIMENTAL

The nanoporous material investigated in the current study was a nanoporous carbon, BP-2000, provided by Cabot (Boston, MA) in powder form, with the particle size of about 50 μm. To minimize the effects of treatment history, the material was dried in air at 80 °C for 2 h, heated in a nitrogen environment at 500 °C for 4 h, and thoroughly rinsed in acetone and warm water three times. The BP2000 powders were then placed in a tube furnace. A saturated water steam flow was maintained at a constant rate of 10 mL/min across the sample for 12 h at 180 °C. After drying, the material was sealed in a round bottom flask with 10 mL of 2.5% dry toluene solution of chlorotrimethylsilane. The mixture was stirred at 90 °C for 4 h in a thermal mantle, followed by repeated rinsing in dry toluene, acetone, and warm water, and vacuum drying at 80 °C for 24 h. By using a Micromeritics ASAP 2000 Gas Absorption Analyzer (Norcross, GA), it was determined that the average nanopore size was 16.7 nm, the nanopore surface area was 1225 m^2/g, and the nanopore volume was 2.1 cm^3/g.

To modify the wettability of the outer surface, immediately after drying, the BP-2000 sample was mixed with 150 mL of dry toluene and 2 g of 16-mercaptohexadecanoic acid (MHA) in a sealed flask. The mixture was stirred at room temperature for 10 min and refluxed at its boiling point for 48 h. A drying tube was attached to the top of the reflux apparatus. The material was then filtered, washed in dry toluene, methanol, and deionized water, and dried in vacuum at 80 °C for 6 h. After the MHA treatment, the material was characterized again by the ASAP-2000 Analyzer. The average nanopore size was 16.3 nm and the specific nanopore volume became 1.4 cm^3/g.

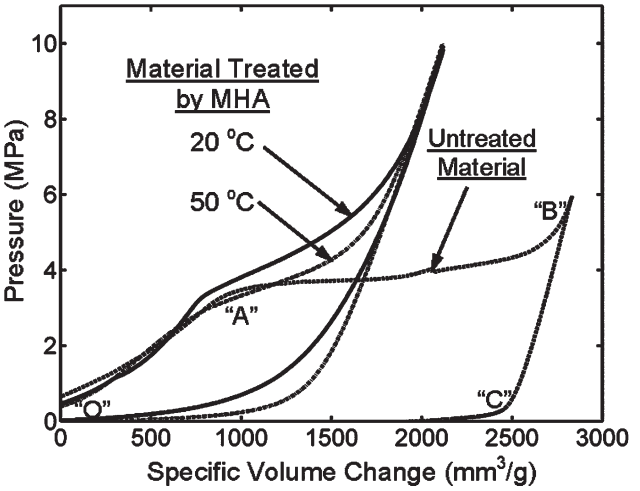

FIG. 1. Typical infiltration curves. The dashed curve indicates the behavior of untreated material.

About 0.3 g of BP-2000 particles, ether treated with MHA or untreated, was mixed with 6 g of saturated aqueous solution of potassium chloride (KCl) in a stainless steel cylinder. A steel piston was intruded into the cylinder by a type 5580 Instron machine (Norwood, MA) at a constant rate of 0.5 mm/min. The cross-sectional area of the piston was 286 mm^2. As will be discussed below, in a certain pressure range, an infiltration plateau could be observed. Once the infiltration was completed, the piston was moved out of the cylinder at the same rate. Figure 1 shows typical sorption isotherm curves, demonstrating the pressure as a function of system volume change. During the testing procedure, the system temperature was controlled by a water bath at either 20 °C or 50 °C.

III. RESULTS AND DISCUSSION

In the silane treatment process, the silane molecules react with the hydroxyl sites at both the inner surfaces of the nanopores and the outer surfaces of the particles, forming $-CH_3$ surface groups.[16] The neutral surface groups repel water molecules, and thus the carbon surface becomes hydrophobic. When the silane treated carbon powders are added in the KCl solution, even after prolonged mixing no stable suspension can be formed. The lightweight carbon particles would rapidly float on the surface, and the clear liquid phase is left below.

As the heterogeneous system is compressed by a quasi-static loading, initially when the pressure is relatively low, the carbon powder layer and the liquid layer deform separately. While the liquid phase is nearly incompressible, the carbon powders are only loosely packed and thus can be condensed easily. The system volume decreases with the increase in pressure (section OA), with the slope of sorption isotherm curve of about 3.75 kPa·g/mm^3. When the pressure is increased to nearly 3.5 MPa, an abrupt transition from the ramp (OA) to a plateau (AB) is observed, which should be attributed to the infiltration of the pressurized liquid into the nanopores. The addition of the electrolyte increases the surface tension of the liquid phase, and thus makes the transition clearer.[17] The plateau is flat, indicating that the effective viscosity of the confined liquid is low, so that the internal friction effect is negligible. The reduction in liquid viscosity at small length scale is associated with the breakdown of the continuum interface structure and the insufficient space for the development of velocity profile.[18] The infiltration continues from A to B, after which the slope of the sorption isotherm curve rapidly increases, indicating that the nanopores are filled. The width of the infiltration plateau is around 1.8 cm^3/g, close to but lower than the gas absorption measurement result of porosity. The difference between the effective nanopore volumes in liquid infiltration and gas absorption tests may be related to the van der Waals distance of water molecules, which is about 0.2–0.3 nm.[19] Immediately next to the large nanopore surface (1225 m^2/g), the inaccessible space is 240 to 360 mm^3/g. Due to the relatively short treatment time, the surface coverage of the silane groups is far from being saturated. If the treatment time is increased to 8 h, the infiltration pressure would be increased by about 20%. As the surface density of the silane groups is relatively low, their influence on the effective pore volume is only secondary.

When the pressure is lowered, the unloading path (BC) does not overlap with the loading path; that is, the sorption isotherm curve is highly hysteretic. The effective compressibility of the system is nearly the same as that at the high-pressure range of the loading path, larger than both of the slopes in sections OA and AB. The effective compressibility should be mainly determined by the machine compliance. Not until the pressure is reduced to about 0.2 MPa does the system volume recovery start to accelerate, forming a defiltration plateau (CO). The difference in the loading and unloading behaviors should be related to the irreversibility of the motion of the confined liquid. Under high pressure, the liquid molecules and ions can overcome the energy barrier among the tetrahedral sites when they slide along the nanopore surface into the interior of a nanoporous particle. During unloading, since no negative pressure difference can be applied, the confined liquid must rely on thermal motion to overcome this internal friction effect, which needs to be aided by additional driving force.[20,21] The required driving force can be estimated as 3.3 MPa, the difference between the infiltration pressure and the defiltration pressure. As an order-of-magnitude assessment, the difference in effective interfacial tensions in infiltration and defiltration is about 13 mJ/m^2, which looks plausible compared with the system free energy variation associated with direct interaction among the liquid and solid molecules.[22]

The molecular formula of MHA is $HS(CH_2)_{15}CO_2H$. The MHA molecules react with the active hydroxyl sites at carbon surfaces and form long chains with negatively charged end groups. The details of the surface reactions on metallic and ceramic materials have been discussed by a number of researchers.[23–25] With such a polar structure, the surface tends to be hydrophilic, opposite to the effect of the silane groups. Since the repelling effect of the neutral CH_3 end of a silane group to water molecules is based on the relatively weak van der Waals interaction while the attraction effect of a charged MHA group is based on the strong hydrogen bond, the latter tends to be dominant. As a result, with the MHA treatment, the carbon surface becomes hydrophilic. As the treated BP-2000 powders are mixed with the liquid, they can be suspended uniformly. After mixing and being at rest for 12 h, no evidence of phase separation can be observed. Clearly, the surface charges keep the carbon particles separate.

If the inner surface modification at the inner surfaces of nanopores is similar to that of the particle outer surface, the inner surface would also be hydrophilic. Under this condition, once the BP-2000 is mixed with the KCl solution, the nanopores would be soaked up spontaneously; and as pressure is applied no further infiltration should be observed. The testing curve in Fig. 1, however, exhibits a clear infiltration plateau, suggesting that the inner surfaces of nanopores are still hydrophobic. An interesting phenomenon is that, with the addition of the hydrophilic MHA groups, the pressure at the onset of infiltration does not vary much. Moreover, as the infiltration continues, the infiltration pressure significantly increases. At the end of infiltration, the pressure is nearly 7.5 MPa, higher than the initial infiltration pressure by more than 100%. The average slope in the infiltration plateau is around 3 kPa·g/mm^3, only slightly smaller than that of the low-pressure section.

While there is no direct experimental method to determine the distribution profile of the surface group density inside the nanopores, since increasing MHA treatment time would not cause detectable changes in the sorption isotherm curve, the treatment effect is saturated. The high degree of hydrophobicity of the inner surface may be attributed to the unique chain configuration in the confining nanoenvironment, as depicted in Fig. 2. In a

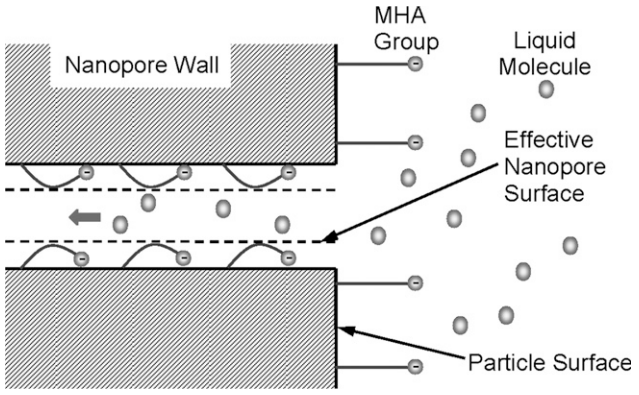

FIG. 2. Schematic of infiltration of liquid phase into a nanopore.

nanopore, along the axial direction, the space is much less constrained than the radius direction. Thus, to minimize the system free energy, the relatively long MHA chains tend to extend along the pore wall, and thus the negatively charged end groups are buried by the nonpolar CH_2 groups. Note that the confinement effect of the nanopore walls on the configuration of silane groups is much less pronounced, since the silane group used in the current study is only around 0.3 nm long, much shorter than MHA. With the long MHA chains, the inner surfaces are of a high effective roughness, and thus when the liquid molecules and ions slide against the solid wall, the energy barrier that they must overcome at tetrahedral sites increases. As a first order approximation, the total internal friction acting on the confined liquid segment can be assumed proportional to the infiltration depth. Thus, as the infiltration volume increases, the pressure that is required to maintain the liquid intrusion rises linearly, as observed in the experiment. For each gram of BP-2000 sample, the additional work that the external pressure does during the infiltration process is around 2.3 J. That is, the energy barrier associated with liquid sliding along inner surface is 1.9 mJ/m^2, or 1.9×10^{-15} $J/\mu m^2$, about 10% of the effective solid-liquid interfacial tension. The increase in infiltration pressure may also be related to the surface charges of MHA groups at the outer surface near the nanopore opening, which form an electric field normal to the liquid transport direction that requires additional work.[26] With the surface groups, the effective nanopore size is smaller, as will be discussed shortly, which may promote the capillary effect, leading to a higher infiltration pressure. However, since these two factors are independent of the infiltration depth, they are secondary compared with the internal friction effect.

The presence of the MHA groups at inner nanopore surfaces is also validated by the gas absorption analysis after the surface treatment. With the decoration of MHA groups, both the nanopore size and the nanopore volume are decreased. From the width of the infiltration plateau, the volume of the nanopores filled by the liquid phase is reduced by almost 35%, to 1.2 cm^3/g. Compared with the untreated material, it is equivalent to a reduction in nanopore radius of about 0.5 nm. This value is much smaller than the MHA chain length (about 4 nm), which, again, implies that the MHA groups extend along the axial direction. The decrease in effective nanopore volume measured in the gas absorption experiment is less pronounced, probably because of the relatively high mobility of gas molecules that can relatively easily penetrate into the space in between adjacent surface groups.

When unloading begins, defiltration occurs at a much lower pressure compared with infiltration, similar to the untreated material. The transition from the linear pressure decrease to the defiltration plateau, however, is much less sharp, indicating that even at a relatively high pressure defiltration can gradually take place, which can be attributed to the complicated configuration change of MHA chains subjected to the pressure variation.

Similar characteristics of infiltration and defiltration can be observed at an elevated temperature. In the temperature range under investigation, the infiltration volume is constant, indicating that the configuration of MHA chains at the inner surfaces does not vary. The liquid suspension is stable; that is, the surface charges at outer surfaces are not significantly affected. However, the infiltration pressure is considerably lowered by about 0.5 MPa, which agrees with previous experimental results on nanoporous silica gels that, when the temperature increase causes a decrease in the liquid surface tension, the effective solid-liquid interfacial tension is also reduced. The difference in infiltration and defiltration pressures is nearly the same, implying again that the MHA configuration, which dominates the energy barrier to the sliding of confined liquid segment along the inner surfaces, is relatively thermal insensitive.

IV. CONCLUSIONS

To summarize, the modification effects of 16-mercaptohexadecanoic acid on the outer and inner surfaces of a nanoporous carbon are considerably different. On the outer surface, the charged MHA chains trigger a hydrophobic-to-hydrophilic transition, so that the carbon particles can be stably suspended in an aqueous solution. On the inner surface, the effective degree of hydrophobicity at the onset of infiltration does not vary much, while as the infiltration continues the required pressure becomes considerably higher. This may be attributed to the anisotropic morphology in the confining nanoenvironment that the charged end groups are buried and the nonpolar chains are exposed to the liquid phase. It agrees with the observation that the infiltration volume decreases after the MHA treatment. These characteristics are not sensitive to the temperature increase, except that the infiltration pressure is lowered.

ACKNOWLEDGMENTS

This study was supported by the National Science Foundation and The Sandia National Laboratory under Grant No. CMMI-0705142, and the William J. von Liebig Foundation.

REFERENCES

1. J.B. Kim, J.W. Grate, and P. Wang: Nanobiocatalysis and its potential applications. *Trends Biotechnol.* **26,** 639 (2008).
2. A. Zukal: Recent trends in the synthesis of nanoporous materials. *Chem. Listy* **101,** 208 (2007).
3. N.Z. Logar and V. Kaucic: Nanoporous materials: From catalysis and hydrogen storage to wastewater treatment. *Acta Chim. Slov.* **53,** 117 (2006).
4. D. Dubbeldam and R.Q. Snurr: Recent developments in the molecular modeling of diffusion in nanoporous materials. *Mol. Simul.* **33,** 305 (2007).
5. S. Polarz and B. Smarsly: Nanoporous materials. *J. Nanosci. Nanotechnol.* **2,** 581 (2002).
6. A. Han, W. Lu, V.K. Punyamurtula, T. Kim, and Y. Qiao: Temperature variation in liquid infiltration and defiltration in a MCM41. *J. Appl. Phys.* **105,** 024309 (2009)**.**
7. A. Han, V.K. Punyamurtula, and Y. Qiao: Effects of cation size on infiltration and defiltration pressures of a MCM-41. *Appl. Phys. Lett.* **92,** 153117 (2008).
8. A. Han, X. Chen, and Y. Qiao: Effects of the addition of electrolyte on liquid infiltration in a hydrophobic nanoporous silica gel. *Langmuir* **24,** 7044 (2008).
9. F.B. Surani and Y. Qiao: An energy absorbing polyelectrolyte gel matrix composite material. *Composites Part A* **37,** 1554 (2006).
10. X. Kong, F.B. Surani, and Y. Qiao: Effects of addition of ethanol on the infiltration pressure of a mesoporous silica. *J. Mater. Res.* **20,** 1042 (2005).
11. L. Liu, Y. Qiao, and X. Chen: Pressure driven water infiltration into carbon nanotube: The effect of applied charges. *Appl. Phys. Lett.* **92,** 101927 (2008).
12. A. Han, V.K. Punyamurtula, T. Kim, and Y. Qiao: The upper limit of energy density of nanoporous materials functionalized liquid. *J. Mater. Eng. Perform.* **17,** 326 (2008).
13. V.K. Punyamurtula, A. Han, and Y. Qiao: An experimental investigation on a nanoporous carbon functionalized liquid damper. *Philos. Mag. Lett.* **86,** 829 (2006).
14. A. Han, V.K. Punyamurtula, and Y. Qiao: Infiltration of liquid metals in a nanoporous carbon. *Philos. Mag. Lett.* **88,** 67 (2008).
15. H. Ibach: *Physics of Surfaces and Interfaces* (Springer, New York, 2006).
16. A. Han and Y. Qiao: Controlling infiltration pressure of a nanoporous silica gel via surface treatment. *Chem. Lett. (Jpn.)* **36,** 882 (2007).
17. A. Han, X. Chen, and Y. Qiao: Effects of the addition of electrolyte on liquid infiltration in a hydrophobic nanoporous silica gel. *Langmuir* **24,** 7044 (2008).
18. X. Chen, G. Cao, A. Han, V.K. Punyamurtula, L. Liu, P.J. Culligan, T. Kim, and Y. Qiao: Nanoscale fluid transport: Size and rate effects. *Nano Lett.* **8,** 2988 (2008).
19. G.X. Cao, Y. Qiao, Q.L. Zhou, and X. Chen: Water infiltration behaviors in carbon nanotubes under quasistatic and dynamic loading conditions. *Mol. Simul.* **34,** 1267 (2008).
20. A. Han, V.K. Punyamurtula, and Y. Qiao: Heat generation associated with pressure induced infiltration in a nanoporous silica gel. *J. Mater. Res.* **23,** 1902 (2008).
21. Y. Qiao, V.K. Punyamurtula, A. Han, X. Kong, and F.B. Surani: Temperature dependence of working pressure of a nanoporous liquid spring. *Appl. Phys. Lett.* **89,** 251905 (2006).
22. J.M. Haile: *Molecular Dynamics Simulation* (John Wiley & Sons, New York, 1992).
23. R. Brito, R. Tremont, O. Feliciano, and C.R. Cabrera: Chemical derivatization of self-assembled 3-mercaptopropionic and 16-mercaptohexadecanoic acids at platinum surfaces with 3-aminopropyltrimethoxysilane: A spectroscopic and electrochemical study. *J. Electroanal. Chem.* **540,** 53 (2003).
24. C.S. Tang, M. Dusseiller, and S. Makohliso: Dynamic, electronically switchable surfaces for membrane protein microarrays. *Anal. Chem.* **78,** 711 (2006).
25. G. Chen, G.T. McCandless, and R.L. McCarley: Integration of large-area polymer nanopillar arrays into microfluidic devices using in situ polymerization cast molding. *Lab Chip* **7,** 1424 (2007).
26. P.C. Hiemenz and R. Rajagopalan: *Principles of Colloid and Surface Chemistry* (Marcel Dekker, New York, 1997).